Study of argon-irradiation-induced defects and amorphization in silicon using a positron beam, Raman spectroscopy and ion channelling

1999 J. Phys.: Condens. Matter 11 5875

(http://iopscience.iop.org/0953-8984/11/30/316)

J. Phys.: Condens. Matter **11** (1999) 5875–5887. Printed in the UK PII: S0953-8984(99)02937-9

Study of argon-irradiation-induced defects and amorphization in silicon using a positron beam, Raman spectroscopy and ion channelling

G Amarendra†§, G Venugopal Rao†, A K Arora†, K G M Nair†, T R Ravindran†, K Sekar‡, B Sundarvel‡ and B Viswanathan†

† Materials Science Division, Indira Gandhi Centre for Atomic Research, Kalpakkam-603 102, India

‡ Institute of Physics, Sachivalaya Marg, Bhubaneswar-751 005, India

E-mail: amar@igcar.ernet.in (G Amarendra)

Received 23 March 1999, in final form 12 May 1999

Abstract. Studies of irradiation-induced defects have been carried out on silicon single-crystal samples, irradiated with 140 keV argon ions to doses in the range 5×10^{14} to 5×10^{16} cm^{-2}, using a variable-low-energy positron beam, Raman spectroscopy and ion channelling. The Doppler broadening lineshape S-parameter has been found to exhibit a peak as a function of the positron beam energy E_p and a subsequent saturation behaviour for all irradiated samples. The peak damage occurs at a depth of 100 nm, consistent with TRIM code calculations. The measured S–E_p curves are analysed using a positron diffusion model to obtain the depth profile of positron-trapping defects. The behaviour of the S–W correlation plots and the variation of the R-parameter indicate that the nature of the open-volume defects is independent of the dose and the dominant defects are vacancy clusters larger than divacancies. Raman spectroscopic studies indicate that all of the irradiated samples are amorphized, and the degree of residual crystallinity across the irradiated zone of the sample is obtained. Ion-channelling studies carried out on the samples have yielded thicknesses of the amorphized layer which are consistent with positron beam results. In contrast to the TRIM code calculations, the present results show the presence of defects at depths far beyond the Ar-ion range. The results of the positron beam, Raman and ion-channelling studies are discussed in the context of ion-induced defects and amorphization.

1. Introduction

The study of ion-beam-induced defects and amorphization in semiconductors has been a subject of both basic and technological interest for a long time [1–3]. Ion beams are particularly useful because by varying the beam energy and its dose, selected depths of the sample can be made disordered or even amorphized [4]. Beyond a critical threshold dose, the implanted layer of the semiconductor crystal is found to turn amorphous, which is understood on the basis of critical defect density (disorder) models of amorphization [5]. Theoretical estimates of the damage profiles have also been made using TRIM code calculations [6] and refined Monte Carlo simulations [7]. In irradiated Si, prior to its amorphization, the divacancies have been found to be the dominant defects [8, 9]. The characterization of defects and disorder in ion-irradiated semiconductors is done using a variety of techniques, such as deep-level transient spectroscopy (DLTS), optical absorption, positron annihilation, Rutherford back

§ Author to whom any correspondence should be addressed.

0953-8984/99/305875+13$30.00

scattering (RBS) and channelling as well as transmission electron microscopy (TEM). Different techniques are sensitive to different types of defect or probe different aspects of the defects. For example, positrons are sensitive to vacancy-like defects in the fractional concentration range 10^{-7} to 10^{-4}, while ion channelling is more sensitive to the interstitial type of defect. On the other hand, the degree of disorder arising due to the snapping of the covalent bonds can be readily quantified using Raman spectroscopy.

Early studies on self-ion irradiation in Si had focused on the estimation of divacancy concentration and the recrystallization during annealing [10]. Recent studies show preferential amorphization in regions with high dislocation density [11]. There have also been positron annihilation studies using different ions such as H [12], F [13], B [14], O [15] and Co [16]. Implantation with heterovalent ions invariably leads to significant doping and consequent changes in electronic properties. Formation of compounds with Si (silicides) due to the dopants has also been reported [16]. There has not been any study using heavy inert-gas ions. Ions heavier than the host atom are known to produce considerably more damage, consisting of bigger defect complexes, as compared to lighter ions. Furthermore, many of the above studies have used only one probe and hence could extract only limited information, focusing only on one aspect of defect formation or annealing. In the present study we use a combination of a low-energy positron beam, ion channelling and Raman spectroscopy to investigate the damage produced by Ar ions in silicon single crystals. In order to produce the damage close to the surface, an energy of 140 keV of the argon ions is chosen. As argon is an inert-gas atom, it is not expected to participate in bonding, and affects the electronic structure of the host only marginally. From the quantitative analysis of the complementary information obtained from these techniques, namely depth-resolved defect parameters from positron annihilation, degree of crystallinity across the sample from Raman spectroscopy and thickness of amorphized layers from ion channelling, we were able to obtain the amorphization/defect profiles through the depth as well as across the irradiated zone of the sample. The critical dose for amorphization obtained in the present studies is also compared with that reported from studies using self-ion irradiation.

2. Experimental details

Single-crystalline Si(111) samples of thickness 0.5 mm are cleaned in a 1:1 solution of hydrofluoric acid and demineralized water. These have been irradiated at room temperature with 140 keV argon ions to doses of 5×10^{14}, 9×10^{14}, 5×10^{15} and 5×10^{16} cm^{-2} using a 150 kV ion implanter. By using a beam collimator, a sample area about $\sim$8 mm in diameter is uniformly irradiated. The samples are mounted on a Cu block of large thermal mass, and low beam currents ($<0.5\ \mu$A) are used for the irradiation. There has not been any appreciable sample heating due to irradiation, owing to the low energy and small beam currents used. A precision current integrator connected to the sample holder is used to obtain the total charge on the sample and in turn the total dose of irradiation. No chemical characterization of the samples as regards surface impurities was carried out after the irradiation. The samples were only cleaned in acetone prior to the experiments. TRIM code [6] calculations have indicated the mean Ar-ion range to be about 175 nm, while the ion-beam-induced damage peaks at around a depth of about 110 nm.

Measurements with variable-low-energy positron beams (LEPB) are carried out on virgin and irradiated Si samples at room temperature using a compact, UHV-compatible and magnetically guided system described earlier [17]. In these experiments, positrons of tunable energy (0–25 keV) are implanted into the sample under study. The implanted positrons become thermalized at around the mean implantation depth, which is determined by the positron beam

energy. Thermalized positrons have a high probability for capture and annihilation at open-volume defects [18, 19]. By measuring the annihilation characteristics in terms of the Doppler broadening of the annihilation 511 keV γ-ray energy, information pertaining to the defects can be obtained. In view of the variable nature of the positron energy, the depth distribution of the defects can be deduced from these experiments. Measurements have been carried out using a slow-positron beam intensity of 4×10^4 e^+ s^{-1}. The positron beam energy E_p is varied from 200 eV to 20 keV in incremental steps so as to probe various sample depths. The mean implantation depth of the positrons, z (nm), is related to the positron beam energy E_p (keV) through the relation [19]

$$z = 40E_p^{1.6}/\rho \tag{1}$$

where ρ is the density of the sample in g cm^{-3}. The Doppler broadening of the annihilation 511 keV γ-ray energy is monitored using a 25%-efficient HPGe germanium detector. The detector is positioned perpendicular to the beam line, and the sample-to-detector separation is about 3 cm. All of the spectra are recorded in the same geometry. A lineshape S-parameter [18, 19], which represents the valence electron annihilation events, is defined as the ratio of the total counts for the energy windows 510.2–511.8 keV (the central-peak region) and 503–519 keV (the photo-peak region). Similarly, the complementary W-parameter, representing the core-electron annihilation events, is defined as the normalized counts in the wing portions of the Doppler broadening curve.

Raman spectroscopy is one of the established methods of semiconductor characterization as regards determining the crystalline structure, disorder and amorphization [20]. The existence of disordered or amorphized layers within its sensitive depth region of $\sim$100 nm can be established from these studies. Raman spectroscopic measurements on unirradiated and irradiated samples have been carried out in the back-scattering geometry at room temperature. The 514.5 nm line of an argon-ion laser is used to excite the Raman spectra. Scattered light from the sample is analysed using a Spex double monochromator and detected using a cooled photomultiplier tube operated in the photon-counting mode [21]. Scanning of the spectra and data acquisition are carried out using a home-built microprocessor-based data-acquisition and control system. Subsequent to the completion of a scan, data are transferred to a personal computer for further analysis. In order to obtain spatially resolved information about the damage profile in the irradiation zone, the laser beam is focused to 50 μm. Raman spectra are measured at close intervals by translating the sample perpendicular to the laser beam using a precision translation stage.

Ion-channelling measurements have been carried out using 2 MeV He ions from a 3 MeV Pelletron accelerator at the Institute of Physics, Bhubaneswar. These investigations have been done on Si samples irradiated with 5×10^{14}, 9×10^{14} and 5×10^{16} Ar cm^{-2} at room temperature. The energy spectrum of the back-scattered He ions has been monitored using a surface barrier detector kept at 150° with respect to the incoming alpha beam. The measurements have been made on the unirradiated portion as well as the irradiated portions of the samples, and the spectra have been normalized to the same charge. The aligned spectrum of the irradiated portion of the samples is compared with the aligned and random spectra of the unirradiated sample so as to bring out evidence for the existence of disorder or amorphization in the irradiated samples [22].

3. Results

3.1. Low-energy positron beam studies

The variation of the normalized S-parameter as a function of the positron beam energy E_p is shown in figure 1 for unirradiated (reference) and irradiated Si samples [23] irradiated to doses

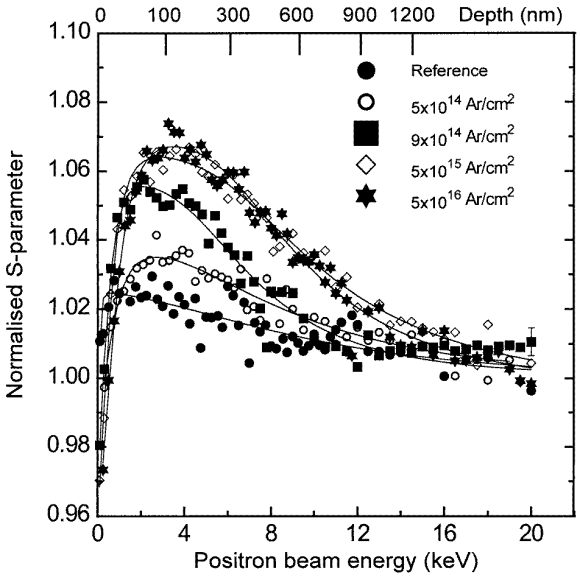

Figure 1. The variation of the normalized S-parameter as a function of the positron beam energy E_p for unirradiated (reference) and irradiated Si(111) samples. The solid curves through the data points are the results from a model analysis using the VEPFIT program. The depth scale probed by the positron beam is indicated on the top axis.

of 5×10^{14}, 9×10^{14}, 5×10^{15} and 5×10^{16} Ar cm^{-2}. The depth probed by the positron beam corresponding to E_p is indicated on the top axis. The solid curves through the data points represent the results of the VEPFIT analysis [24] based on an assumed box profile for the defect distribution, which will be discussed later. As compared with those for the reference sample, the observed changes in the S–E_p curves for the irradiated samples can be summarized as follows:

(a) The S-parameter increases from the surface and shows a maximum at around $E_p \sim$ 3.5 keV, beyond which it gradually decreases and matches with that of the reference sample.
(b) The height of the S–E_p curves progressively increases as the dose is increased and shows saturation behaviour beyond 5×10^{15} Ar cm^{-2}.
(c) The widths of the S–E_p curves are smaller for the low-dose samples as compared to those for high-dose samples.

These results can be explained as follows. The observed increase in the S-parameter as a function of E_p indicates that the concentration of the positron-trapping defects increases as the beam travels through the depth of the sample. The position of the maximum S-parameter signifies the depth of the peak damage layers in the samples. As seen from figure 1, this is found to be 100 nm, which compares favourably with 110 nm for the maximum of the vacancy profile as calculated from the TRIM code [6]. The increase in the maximum value of the S-parameter with increasing dose signifies that the total positron trapping rate in the irradiated region is increasing. This could occur due to increase in either the concentration of the defects or their size. The saturation behaviour of the S-parameter beyond the 5×10^{15} Ar cm^{-2} dose indicates that the ion-induced defect concentration is sufficiently large that saturation positron

trapping is exhibited. The observed increase in the widths of the S–E_p curves indicates that the spatial distribution of the irradiation-induced defects has broadened. These aspects are discussed below in more detail.

The experimental S–E_p curves have been analysed on the basis of the positron diffusion model using the VEPFIT program [24]. In this model analysis, positrons may annihilate with contributions from surface, epithermal, defect and bulk states. Hence, the measured S-parameter at a given E_p can be expressed as

$$S(E_p) = f_{ep}S_{ep} + (1 - f_{ep})\{f_sS_s + f_dS_d + f_bS_b\} \tag{2}$$

where S_{ep}, S_s, S_d and S_b are the characteristic S-parameters corresponding to the epithermal, surface, defect and bulk states respectively, while f_{ep}, f_s, f_d and f_b are the probabilities of positron annihilation in these states respectively. For the case of the reference sample, i.e., the unirradiated sample, the term corresponding to the defect is not included, while for all of the irradiated samples, it is included. Using the VEPFIT program, one could delineate the annihilation parameters corresponding to various positron states and also deduce the depth distribution of defects on the basis of a comparison of the fitted and experimental S–E_p curves. S_d for the irradiated samples, normalized with respect to S_b for the unirradiated sample, as obtained from VEPFIT analysis is shown in figure 2 as a function of the irradiation dose. As can be seen from figure 2, the S_d-value increases as the irradiation dose is increased and tends to saturation. The saturation behaviour, beyond a dose of 5×10^{15} Ar cm^{-2}, indicates that all of the positrons are trapped at defects, leading to saturation positron trapping.

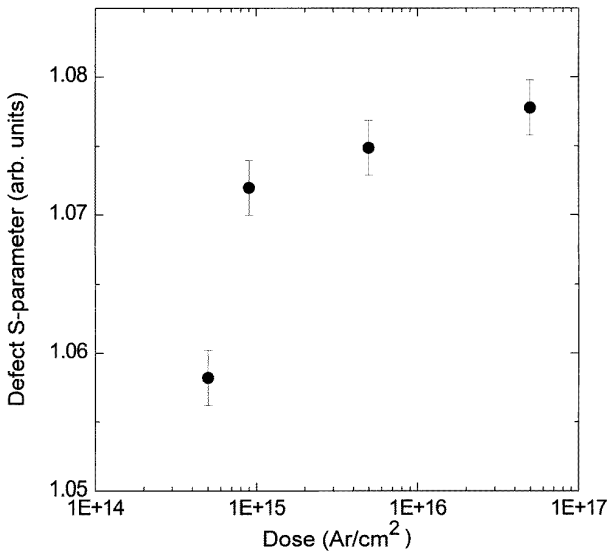

Figure 2. The normalized S-parameter corresponding to the defect layer S_d versus the Ar-ion dose.

We now address the identification of defects in the irradiated samples. At the outset, certain inferences can be drawn as regards the nature of the defects in the damaged layers by comparing the values of S_d and S_b. The resolved defect parameter S_d for divacancies in Si is reported [25] to have a value of 1.046 ($S_d = 1.046S_b$). In the present positron beam studies, we have observed S_d-values in the region of 1.058 even for the lowest-dose sample, which implies that the irradiation-induced defects are vacancy clusters bigger than divacancies. In

recent studies [26], the R-parameter, defined as

$$R = (S_d - S_b)/(W_b - W_d) \tag{3}$$

which is independent of the defect concentration, has been employed to identify the defects in irradiated semiconductors. For the sample with a dose of 5×10^{14} Ar cm^{-2}, we deduce a value of 4.56 ± 1.02 for the R-parameter and this remains unchanged for all other irradiated samples within the experimental error. It may be mentioned that this is significantly larger than the characteristic value of 1.8 reported for monovacancies in semiconductors [26]. This leads to the inference that the size of the defect in the damaged layers of Si is larger than that of a single vacancy or divacancy. Positron lifetime experiments, using a LINAC-based intense positron beam [27], carried out on the high-dose sample have exhibited a typical lifetime value of 380 ps in the peak damage regions [28]. This value is larger than the divacancy value ($\sim$325 ps) and smaller than the four-vacancy-cluster value ($\sim$435 ps) [25]. On the basis of this, it is plausible that the defect clusters are mostly trivacancy clusters. Apart from the resolved S-parameter and R-parameters, correlation plots of S- and W-parameters [16, 26] have also been used recently for identification of defects in semiconductors. In these plots, the W-parameter is plotted as a function of the S-parameter with the positron beam energy being the implicit parameter. As the positron probes progressively varying depths, the positron annihilates only at the surface and bulk states (in the absence of defects). This results in an inverse linear relationship between the W-parameter and S-parameter in an S–W correlation plot; i.e., as the W-parameter increases (decreases), the S-parameter decreases (increases). The presence of defects would alter this relationship and result in a curved plot. For example, the presence of native defects in GaAs is reported to lead to a triangular plot [26]. The shape of the plot could also change according to the nature of the defects. Thus, the S–W correlation plots are useful for obtaining information about the existence and any change in the nature of defects. The experimental S-parameter data shown in figure 1 together with the complementary W-parameter data have been used to construct S–W correlation plots. Figure 3 shows these representative plots for the samples irradiated with the lowest and the highest dose. Note that the samples exhibit similar triangular plots, each with a vertex. This implies that the natures of the defects are the same in low- and

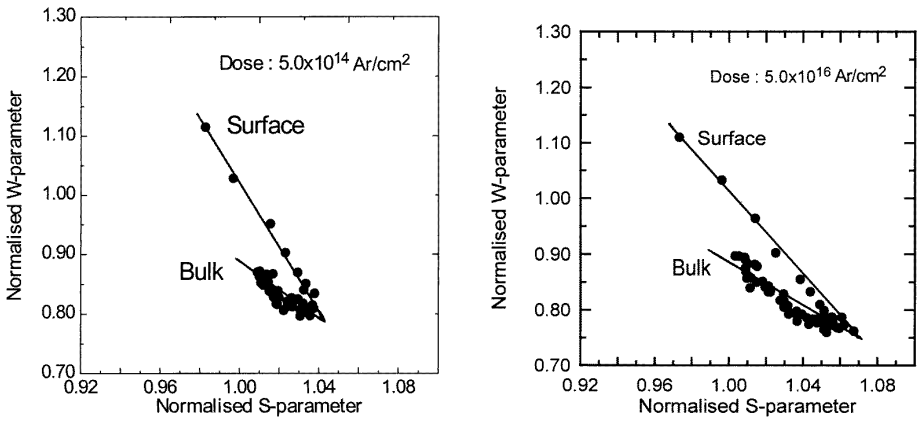

Figure 3. S–W correlation plots for samples irradiated with doses of (a) 5×10^{14} Ar cm^{-2} and (b) 5×10^{16} Ar cm^{-2}. In these plots, the positron beam energy E_p is the variable and implicit parameter.

high-dose samples. Thus, the S–W correlation plots reveal that the natures of the positron-trapping defects in all of the irradiated samples are similar. On the basis of the observed values of the normalized S- and R-parameters, these defects seem to be bigger than divacancies and are likely to be trivacancy clusters.

We discuss here the possibility of the implanted Ar ions clustering with irradiation-induced vacancies to give rise to Ar bubbles, which could be acting as positron-trapping defects in the irradiated samples. As is evident from the TRIM code calculations, the mean stopping range of 140 keV Ar ions in Si is about 175 nm. If Ar bubbles were to have formed, these could be expected to be present only at greater depths in the sample of around 175 nm and not from the sample surface downwards. As is evident from the experimental S–E_p curves, the presence of the defects is observed right from the sample surface, peaking at a depth of about 100 nm and progressing further to greater depths. Therefore, the present experimental observations cannot be explained on the basis of the formation of Ar bubbles, even though their occurrence cannot be ruled out.

We discuss now the defect distribution in the damaged layers. As mentioned earlier, the experimental S–E_p curves shown in figure 1 have been fitted using positron diffusional model analysis, wherein a defect profile of some assumed width has been taken to be a box profile for the sake of simplicity. The width of the box profile is varied so as to obtain a best fit to the experimental data. The defect concentration profiles that have been deduced from the fitting are shown in figure 4. The widths of these defect-containing layers are found to be 250, 325, 500 and 525 nm (with an error bar of ± 50 nm) for the samples irradiated to doses of 5×10^{14}, 9×10^{14}, 5×10^{15} and 5×10^{16} Ar cm^{-2} respectively. The error bar is typical for positron diffusion lengths in defect-containing layers. The deeper damage seen at higher irradiation doses is consistent with earlier observations [3]. For the lowest-dose sample, the estimated width of the defect profile is 250 nm, which matches well with that from the TRIM code [6],

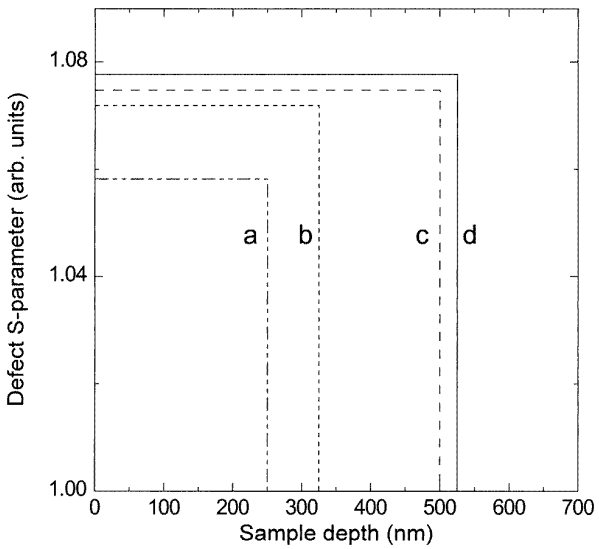

Figure 4. The box profile of the defects used in the VEPFIT program for fitting the experimental data shown in figure 1. Curves a, b, c and d correspond to Ar doses of 5×10^{14}, 9×10^{14}, 5×10^{15} and 5×10^{16} Ar cm^{-2}, respectively.

which gives a value of 260 nm. However, the depth range over which the defects are found to be present in the higher-dose samples is much larger than the value calculated using the TRIM code. This discrepancy may possibly be due to the following facts:

(a) The TRIM code, which is basically a zero-temperature calculation for an amorphous host matrix, does not take into account the mobility and clustering of defects as well as the channelling effects of ions during the irradiation. It is known that at room temperature, monovacancies are mobile which could diffuse deeper and cluster, thereby leading to the spreading of the damage to much deeper layers.
(b) Positron annihilation techniques are sensitive to the fractional defect concentration down to 10^{-7} and thus could pick up the presence of the diffused defects in the deeper layers. There have been earlier reports [13] wherein the presence of defects is detected far beyond the depths calculated by the TRIM code.

Finally, it should be pointed out that the positron beam experiments cannot reveal whether the irradiated samples are disordered crystalline or amorphous. Furthermore, the positron beam diameter used in the present experiments is comparable to that of the irradiation zone of the samples. Hence, the lateral distribution of defects across the irradiated zone of the samples also could not be determined. These aspects are discussed below.

3.2. Raman spectroscopic studies

Raman spectroscopic measurements have been carried out on the unirradiated and irradiated Si samples [29]. In order to obtain spatially resolved information about the defects and disorder across the irradiated zone, Raman measurements are carried out with the laser beam focused down to 50 μm. Figure 5 shows the Raman spectra for the unirradiated Si and Si irradiated to a dose of 5×10^{15} Ar cm^{-2}. The sharp peak seen in the spectra at around 520 cm^{-1} for the unirradiated sample shown in figure 5(a) corresponds to the transverse optic (TO) phonon of crystalline Si. As a result of the irradiation, the Si–Si bonds break and disorder sets in in the matrix. This leads to a reduction in the intensity of the crystalline peak. In addition, a broad band appears, centred at around 480 cm^{-1}. This represents the phonon

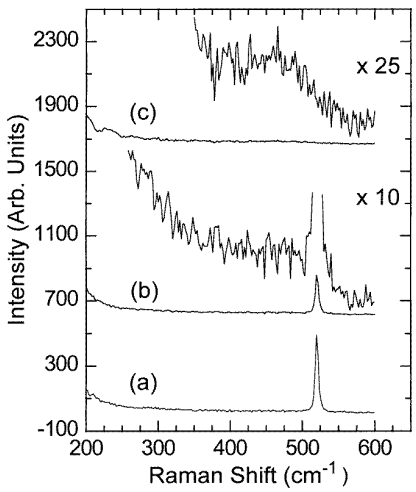

Figure 5. Raman spectra for (a) an unirradiated (reference) Si sample, (b) the edge of the irradiated zone and (c) the central portion of the irradiated zone corresponding to a sample irradiated with 5×10^{15} Ar cm^{-2}. Spectra (b) and (c) are vertically displaced for the sake of clarity. The magnifications used are indicated.

density of states, which becomes observable in the Raman spectra due to the relaxation of the zero-scattering-vector selection rule for a disordered system. However, when the irradiation-induced defect concentration is sufficiently large, the crystalline structure is no longer stable and becomes amorphous. This leads to the complete disappearance of the crystalline peak and this can be considered as a signature of complete amorphization of the implanted layers. Figure 5(b) corresponds to the Raman spectrum taken towards the edge of the irradiated zone. As compared to the intensity of the unirradiated region, the intensity of the crystalline peak is considerably lower and is accompanied by a weak broad maximum at 480 cm^{-1}. This suggests that towards the edge of the irradiated region, the sample exhibits only partially amorphization, coexisting with a disordered crystalline matrix. On the other hand, the Raman spectrum, shown in figure 5(c), taken in the central region of the irradiated zone now contains only the broad band, which indicates that the sample is completely amorphous. The inhomogeneous damage distribution inferred from Raman measurements—namely the central irradiation zone being completely amorphous while the edges have partial crystallinity—may arise from the spatially inhomogeneous profile of the 140 keV argon-ion beam used for the irradiation. In view of the large size of the ion beam (∼8 mm diameter) used for the irradiation, it is possible that there is spatial variation of the flux across the diameter of the irradiated zone. In order to quantify this, the focused laser spot has been scanned across the diameter of the irradiated zone and the Raman spectra have been recorded at close intervals. The measured spectra are least-squares fitted to a Lorentzian lineshape for the 520 cm^{-1} TO phonon peak and the 480 cm^{-1} broad band, along with a suitable background. The area under the 520 cm^{-1} peak, when normalized to that of the unirradiated region, is taken as a measure of the residual crystallinity of the sample. The residual crystallinity thus obtained is shown in figure 6 as a function of the lateral position in the irradiated zone for the sample irradiated with a dose of 5×10^{14} Ar cm^{-2}. In the central portion of the irradiated zone, the sample is completely amorphized. Due to

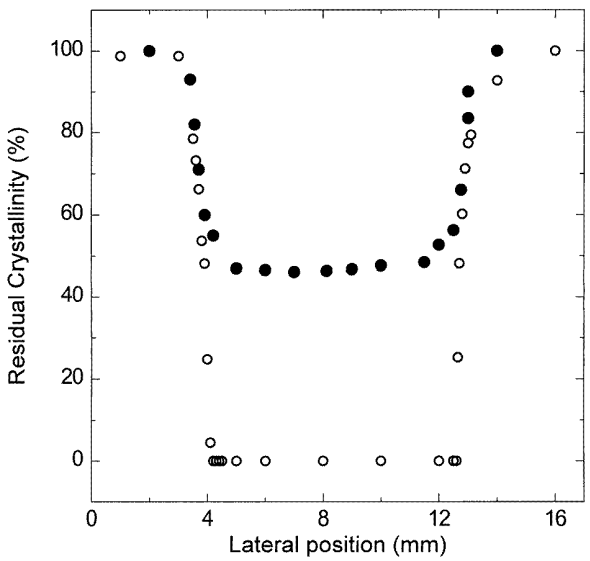

Figure 6. Residual crystallinity (%) as a function of lateral position in the irradiated zone (∼8 mm) for samples irradiated with 5×10^{14} Ar cm^{-2} (open circles) and 5×10^{13} Ar cm^{-2} (filled circles). The variation of the intensity of the 520 cm^{-1} crystalline peak has been used to obtain this plot.

the non-uniform irradiation conditions, a varying degree of crystallinity is seen only at the edges. Similar features were observed for all other irradiated samples. As the lowest dose, i.e., 5×10^{14} Ar cm^{-2}, gives rise to complete amorphization, in order to obtain the critical dose for amorphization, irradiation at a dose lower than this was also carried out. Due to experimental difficulties, only Raman spectroscopic measurements could be carried out on this sample irradiated with 5×10^{13} Ar cm^{-2}. Figure 6 also shows the residual crystallinity profile for this sample. Note that the degree of residual crystallinity is about 50%, suggesting that the critical dose for amorphization of Si with Ar ions is of the order of 5×10^{13} Ar cm^{-2}. This is significantly lower than the critical dose of 2×10^{15} cm^{-2} for the MeV self-ion irradiation in Si. In view of the heavier mass of the Ar ion, which produces more extensive damage, the lowering of the threshold dose is understandable. It should be emphasized that Raman studies would only reveal the existence of either disordered or amorphized layers of the samples within the skin depth of the laser wavelength in Si, which is about 100 nm. Thus, information as regards the width of the amorphized layers cannot be obtained by this technique.

3.3. Ion-channelling studies

In order to obtain independent evidence of amorphization and an estimate of the widths of the amorphized layers, ion-channelling studies [30] have been carried out on the same irradiated samples. Figure 7 shows the back-scattered yield as a function of channel number for Si samples irradiated to doses of 5×10^{14}, 9×10^{14} and 5×10^{16} Ar cm^{-2}. The aligned and random spectra of unirradiated Si are also shown. In ion-channelling experiments, the presence

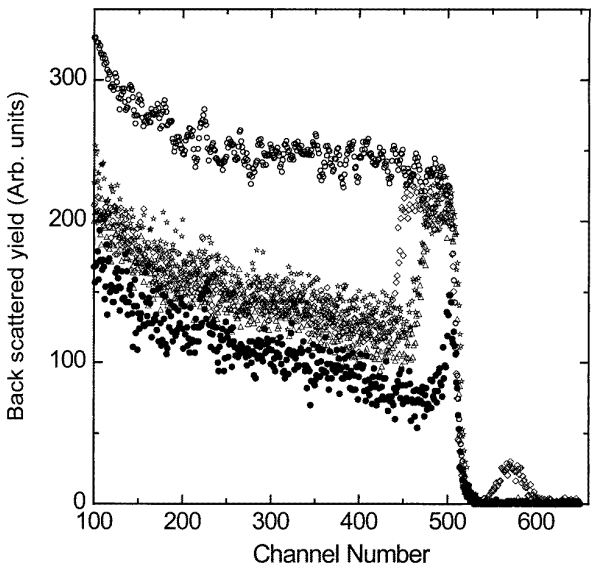

Figure 7. Back-scattered yield versus channel number deduced from ion-channelling studies for virgin Si in aligned (closed circles) and random (open circles) configurations and for samples irradiated to 5×10^{14} Ar cm^{-2} (stars), 9×10^{14} Ar cm^{-2} (triangles) and 5×10^{16} Ar cm^{-2} (diamonds). The sharp peak seen in the aligned spectrum of the virgin sample, around channel number 500, corresponds to the surface peak. The small peak seen in the high-dose sample spectrum around channel number 575 corresponds to Ar.

of a disordered region is manifested in the spectra as an increase in the yield over a certain energy range, which corresponds to the thickness of the disordered region. The disorder present in the crystalline matrix will exhibit a yield in between the random and aligned yields. On the other hand, when the layer under consideration is amorphous, the measured yield matches the random yield [22]. An examination of the spectra in figure 7 shows that even the sample irradiated with the lowest dose contains an amorphous layer, since the corresponding backscattered yield (channel numbers from 475 to 510) matches the random yield. Furthermore, all of the samples are amorphized from the surface to a certain depth, depending on the dose. The thickness of the amorphous layer can be estimated from the width of the channelling curve from the calculations of the stopping power and energy loss of He ions in the Si matrix [22, 30]. The amorphous layer thickness is found to be 180 ± 20 nm for the two low-dose samples and 320 ± 20 nm for the high-dose sample.

4. Discussion

Positron beam studies have indicated the presence of open-volume defect clusters in all of the irradiated samples and the natures of these defects are found to be similar. Raman spectroscopic and ion-channelling studies have given evidence that these samples are amorphous. Thus, these defects, which act as positron-trapping centres, can be ascribed to the average 'open-volumeness' present in the ion-beam-induced amorphized state of Si. On the basis of the experimental *S*-parameter and *R*-parameter values, the average size of this 'open-volumeness' is found to be larger than that for divacancies. Furthermore, the increase in the *S*-parameter upon increasing the irradiation dose could be ascribed to the increase in the amorphous fraction, which enhances the total positron trapping rate at the defect clusters. The saturation behaviour observed for the *S*-parameter beyond the dose of 5×10^{15} Ar cm^{-2} occurred because the fractional concentration of these positron-trapping centres had increased beyond 10^{-4}, at which concentration all of the positrons are trapped at defect clusters.

As regards the estimation of the widths of the defect-containing or amorphous layer in the irradiated samples, for the lowest-dose sample, the estimates derived using the positron beam (250 ± 50 nm) and ion channelling (180 ± 20 nm) are comparable with those from the TRIM code calculations ($\sim$260 nm). On the other hand, for the high-dose sample with 5×10^{16} Ar cm^{-2}, the width of the amorphous layer deduced from the channelling studies is $\sim$320 nm, while the defect profile deduced using positrons indicates the presence of open-volume defects to a depth of $\sim$525 nm. As discussed earlier, the TRIM code has certain limitations as regards estimating the defect profiles for the high-dose samples. The difference between the positron beam and channelling estimates may be attributed to the fact that the concentration of vacancies at greater depths tails off to low values of the order of a few ppm, which is below the detection limit of the ion-channelling technique. On the other hand, the positron annihilation technique has a higher sensitivity for the detection of open-volume defect concentrations in the sample as compared to that of the ion-channelling technique. Thus, positron beam studies have indicated the presence of open-volume defects to much greater depths as compared to channelling studies.

5. Summary and conclusions

The argon-ion-irradiation-induced defects and amorphization of Si samples have been investigated using a low-energy positron beam, Raman spectroscopy and ion channelling. In view of their sensitivity to and selectivity as regards open-volume defects and their depth-

resolved nature, positron beam studies have provided vacancy-specific information as a function of depth for the irradiated samples. The depth of the peak damage region found from the positron S–E_p curves is in agreement with the calculations with the TRIM code. The experimental S-parameter is analysed in terms of the positron diffusion model to deduce the defect profile in the samples. The S–W correlation plots have revealed that the natures of the positron-trapping defects in all of the irradiated samples are the same. These defects are inferred to be vacancy clusters which are larger than divacancies. The near-surface layers are found to be amorphized. The evidence for amorphization has been found from Raman spectroscopic studies, which show that all of the samples with doses above 5×10^{14} Ar cm^{-2} are amorphized. The critical dose for amorphization is found to be of the order of 5×10^{13} Ar cm^{-2}. The widths of the amorphized layers in these samples has been found from the ion-channelling studies, which gave corroborative evidence for the amorphization in the samples. Furthermore, the width of the amorphized layer for the low-dose sample, deduced from the channelling studies, is consistent with the defect profile obtained from the positron beam experiments. For the high-dose samples, positron beam studies have indicated the existence of vacancy-type defects at depths beyond that of the amorphized layer deduced from the channelling studies.

Acknowledgments

The authors would like to thank Dr Shikha Verma of Institute of Physics, Bhubaneswar, for her cooperation in carrying out the ion-channelling experiments. The authors would also like to thank Drs R Suzuki, T Ohdaira, A Uedono and Professor P G Coleman for many useful discussions.

References

[1] Baruch P (ed) 1965 *Radiation Damage in Semiconductors* (Paris: Dunod)
Bourret A 1985 *13th Int. Conf. on Defects in Semiconductors* ed L C Kimerling and J M Parsey Jr (Warrendale, PA: The Metallurgical Society of the AIME) p 129
[2] Henkel T, Heera V, Kogler R, Skorupa W and Seibt M 1997 *J. Appl. Phys.* **82** 5360
[3] Nakata J 1997 *J. Appl. Phys.* **82** 5433
Nakata J 1997 *J. Appl. Phys.* **82** 5446
[4] Williams J S, Elliman R G and Ridgway M C (ed) 1996 *Ion Beam Modification of Materials* (Amsterdam: North-Holland)
[5] Riviere J P 1977 *Radiat. Eff.* **33** 21
Fecht H J 1992 *Nature* **356** 133
[6] Ziegler J F, Biersack J P and Littmark U 1985 *The Stopping and Range of Ions in Solids* (New York: Pergamon)
[7] Lulli G, Albertazzi E, Bianconi M, Nipoti R, Cervera M, Carnera A and Cellini C 1997 *J. Appl. Phys.* **82** 5968
[8] Corbett T, Karins J P and Tan T Y 1981 *Nucl. Instrum. Methods* **182+183** 457
[9] Stein J, Vook F L, Brice D K, Borders J A and Peraux S T 1970 *Radiat. Eff.* **6** 19
[10] Simpson P J, Vos M, Mitchell I V, Wu C and Schultz P J 1991 *Phys. Rev.* B **44** 12 180
[11] Goldberg R D, Williams J S and Elliman R G 1999 *Phys. Rev. Lett.* **82** 771
[12] Fujinami M, Suzuki R, Ohdaira T and Mikado T 1998 *Phys. Rev.* B **58** 12 559
[13] Fujinami M and Chilton N B 1993 *J. Appl. Phys.* **73** 3242
Szeles Cs, Nielsen B, Asoka-Kumar P, Lynn K G, Anderle M, Ma T P and Rubloff G W 1994 *J. Appl. Phys.* **76** 3403
[14] Uedono A, Kitano T, Hamada K, Moriya T, Kawano T, Tanigawa S, Suzuki R, Ohdaira T and Mikado T 1997 *Japan. J. Appl. Phys.* **36** 2571
[15] Fujinami M 1996 *Phys. Rev.* B **53** 12 047
[16] Knights A P, Carlow G R, Zinke-Allmang M and Simpson P J 1996 *Phys. Rev.* B **54** 13 955
[17] Amarendra G, Viswanathan B, Venugopal Rao G, Parimala J and Purniah B 1997 *Curr. Sci.* **73** 409
[18] Brandt W and Dupasquier A (ed) 1983 *Positron Solid State Physics* (Amsterdam: North-Holland)
[19] Schultz P J and Lynn K G 1988 *Rev. Mod. Phys.* **60** 701

[20] Crowder B L, Smith J E Jr, Brodsky M H and Nathan M I 1971 *2nd Int. Conf. on Ion Implantation in Semiconductors* ed I Ruge and J Graul (Berlin: Springer) p 255
Contreras G, Tapfer L, Sood A K and Cardona M 1985 *Phys. Status Solidi* b **131** 475
[21] Arora A K and Sakuntala T 1992 *J. Phys.: Condens. Matter* **4** 8697
[22] Chu Wei-Kan, Mayer J W and Nicolet M-A 1978 *Backscattering Spectrometry* (New York: Academic) pp 223–273
Tesmer J R and Nastasi M (ed) 1995 *Handbook of Modern Ion Beam Materials Analysis* (Pittsburgh, MA: Materials Research Society)
[23] Amarendra G, Venugopal Rao G, Nair K G M and Viswanathan B 1997 *Mater. Sci. Forum.* **255–257** 650
[24] Van Veen A, Schut H, de Vries J, Hakvoort R A and Ijpma M R 1990 *Slow Positron Beams for Solids and Surfaces* ed P J Schultz, G R Massoumi and P J Simpson (New York: American Institute of Physics) p 171
[25] Asoka-Kumar P, Lynn K G and Welch D O 1994 *J. Appl. Phys.* **76** 4935
Nielsen B, Holland O W, Leung T C and Lynn K G 1993 *J. Appl. Phys.* **74** 1636
[26] Liszkay L, Corbel C, Baroux L, Hautojarvi P, Baylan M, Brinkman A W and Tatarenko 1994 *Appl. Phys. Lett.* **64** 1380
Rauhala E, Ahlgren T, Vakevainen K, Raisanen J, Keinonen J, Saarinen K, Laine T and Likonen J 1998 *J. Appl. Phys.* **83** 738
[27] Suzuki R, Kobayashi Y, Mikado T, Ohgaki H, Chiwaki M, Yamazaki T and Tomimasu T 1991 *Japan. J. Appl. Phys.* **30** L532
[28] Amarendra G and Suzuki R 1998 unpublished data
[29] Venugopal Rao G, Amarendra G, Arora A K, Ravindran T R, Nair K G M and Viswanathan B 1997 *Laser Applications in Materials Science and Industry* ed R Kesavamoorthy, A K Arora, C Babu Rao and P Kalyanasundaram (New Delhi: Allied) p 138
[30] Amarendra G, Sundarvel B, Sekar K and Nair K G M 1997 *Proc. DAE: Solid State Physics Symposium (India)* C **40** 172